14.4 Improved Algorithms for Combining Satellite Imagery and Geographic Basemaps

Richard A. Kohrs*
University of Wisconsin, Madison, Wisconsin

1. Introduction

Traditional algorithms for combining satellite imagery with topographic or vegetation basemaps have been limited to using infrared data. Here, an infrared brightness temperature (T_{ir}) is chosen to determine a cloud/no cloud threshold. The product created displays a basemap where T_{ir} is greater than the threshold and infrared satellite data where T_{ir} is less than the threshold. Additionally, a temperature-based transparency is assigned to the satellite data, where colder clouds are more opaque. This method exaggerates cloud coverage over polar regions and underestimates stratiform cloud coverage over lower latitudes. More recently, we have begun to see visible imagery combined with basemaps using an albedo-based transparency. This method greatly improves overall cloud cover estimation, but is limited to daylight hours.

The Datacenter at the University of Wisconsin-Madison generates global real-time weather graphics from its databases of satellite imagery, conventional data and numerical model output. Our first attempts at combining satellite images with basemaps on a global scale accentuated the problems of the traditional algorithm, making our products unacceptable to some of our clients. We have now implemented an algorithm that utilizes surface temperature (T_{sfc}). The value T_{sfc}-T_{ir} determines cloud transparency. Additionally, a second algorithm is described which uses day/time weighting functions to blend visible and infrared data imagery. Examples of both algorithms can be viewed at the following web locations:

http://www.ssec.wisc.edu/~rickk/temp_diff.html
http://www.ssec.wisc.edu/~rickk/vis_ir.html

2. Utilizing Surface Temperatures

The traditional T_{ir} based cloud/no cloud algorithm raised two major concerns with our global satellite products. First, and most important, was the exaggeration of cloud coverage in higher latitudes and second, the loss of warmer stratiform clouds. To address the first issue, we chose to draw upon the simple assumption that $T_{ir}<T_{sfc}$ over cloudy regions and $T_{ir}=T_{sfc}$ over cloud-free regions. Initial tests of our assumption were completed over the continental U.S. and adjacent coastal regions. Using Man computer Interactive Data Access System (McIDAS) software (Lazzara et al. 1999), we created 8-bit calibrated images of T_{ir} (derived from GOES-12 11 μm data), T_{sfc} (analysis derived from surface, ship and buoy observations) and temperature difference, T_{sfc}-T_{ir}. Finally, cloud/no cloud masks, using various values of T_{sfc}-T_{ir} were applied to GOES-12 11 μm data and the results were compared to corresponding GOES-12 visible images. The process is illustrated in Figures 1-9 using 18 UTC data from 29 November 2004. This test case was chosen due to the extreme temperature contrast across the geographical domain.

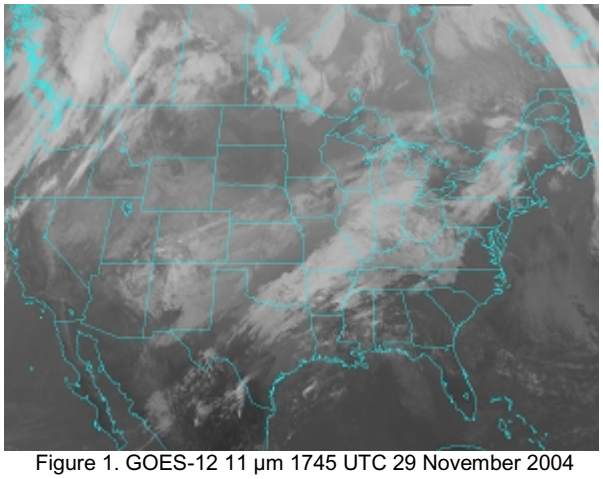

Figure 1. GOES-12 11 μm 1745 UTC 29 November 2004

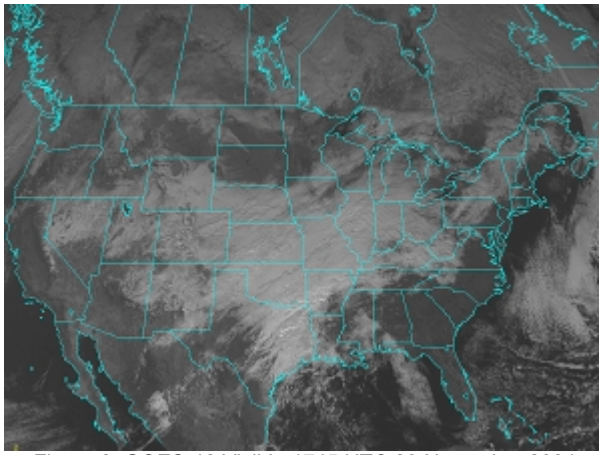

Figure 2. GOES-12 Visible 1745 UTC 29 November 2004

* Corresponding author address: Richard A. Kohrs, Space Science and Engineering Center, University of Wisconsin-Madison, 1225 West Dayton Street, Madison, WI 53706; e-mail rick.kohrs@ssec.wisc.edu

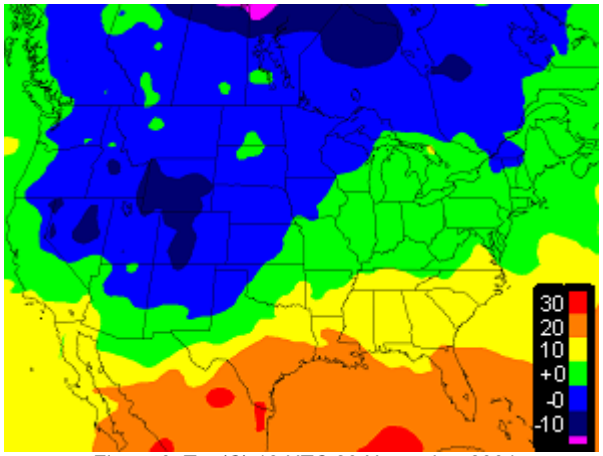

Figure 3. T_{sfc} (C) 18 UTC 29 November 2004

Figures 4-6 show T_{sfc}-T_{ir} masks of 0, 4 and 8 applied the GOES-12 11 µm image. For comparison, three T_{ir} masks (285K, 275K and 265K) are shown in Figures 7-9.

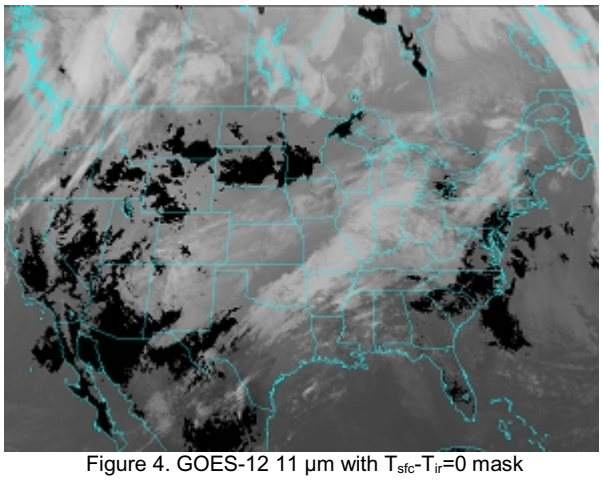
Figure 4. GOES-12 11 µm with T_{sfc}-T_{ir}=0 mask

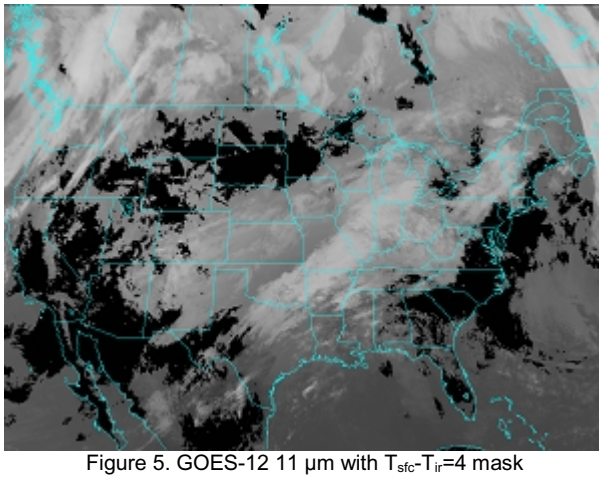
Figure 5. GOES-12 11 µm with T_{sfc}-T_{ir}=4 mask

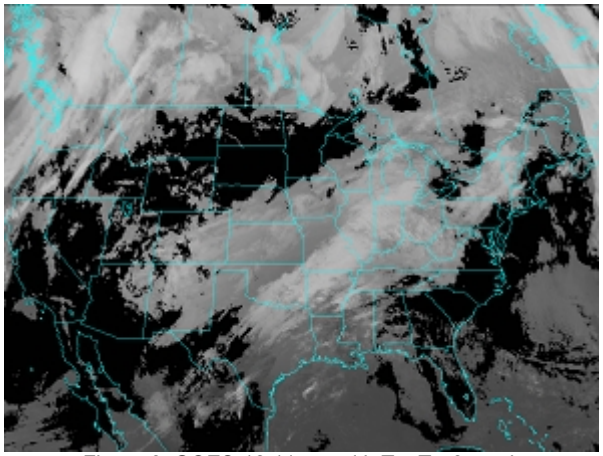
Figure 6. GOES-12 11 µm with T_{sfc}-T_{ir}=8 mask

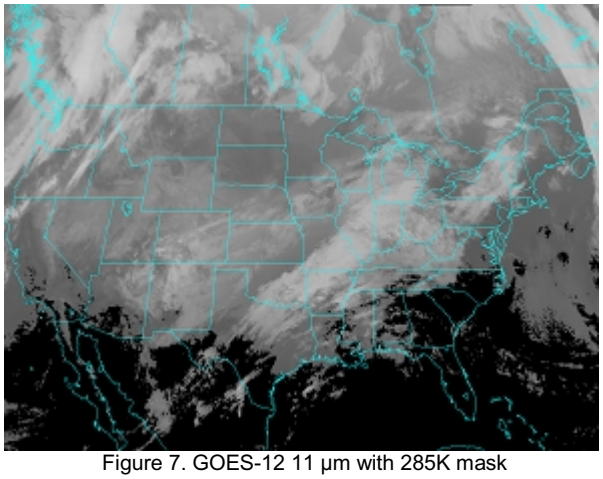
Figure 7. GOES-12 11 µm with 285K mask

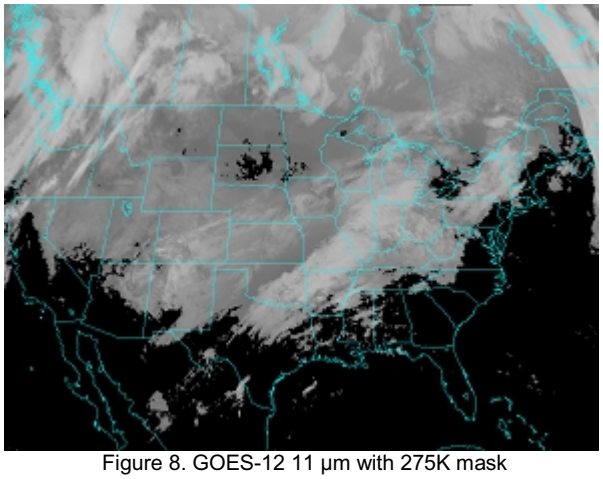
Figure 8. GOES-12 11 µm with 275K mask

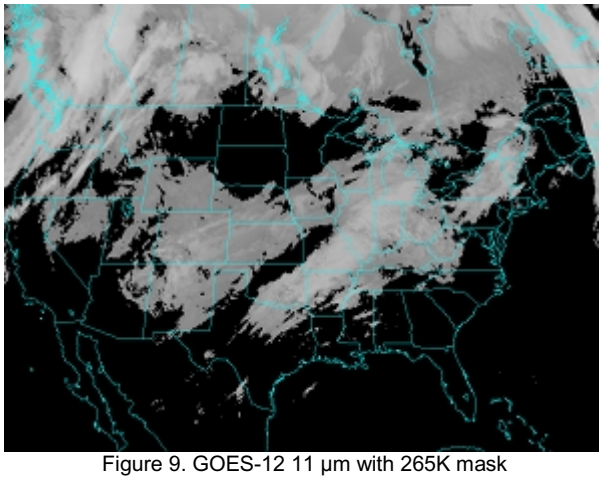

Figure 9. GOES-12 11 μm with 265K mask

Using the visible image as a benchmark, we find that temperature differences masks clouds better than a single infrared temperature threshold. Also, of the three difference thresholds, T_{sfc}-T_{ir}=8 gives the best map.

3. Global Scale

Encouraged by our regional results, we extended our tests globally. Limited observational data over oceanic regions led to poor global T_{sfc} analyses. To rectify this problem, a land/sea mask was implemented enabling us to use 6-hourly synoptic observations over land and daily Reynold's blended sea surface temperature (SST) analysis (Reynolds 1988; Reynolds and Marisco 1993) available from the National Center for Environmental Prediction (NCEP), over oceanic regions (See Figures 10-12).

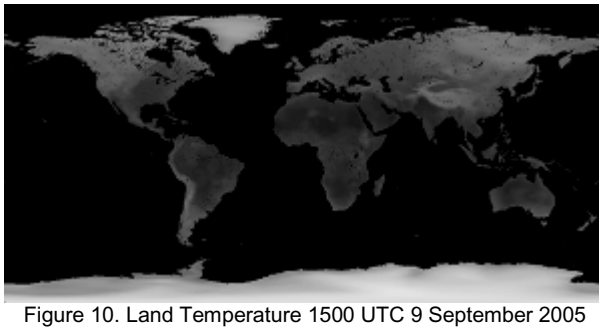

Figure 10. Land Temperature 1500 UTC 9 September 2005

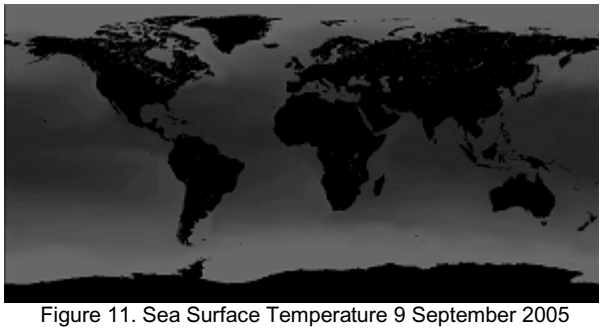

Figure 11. Sea Surface Temperature 9 September 2005

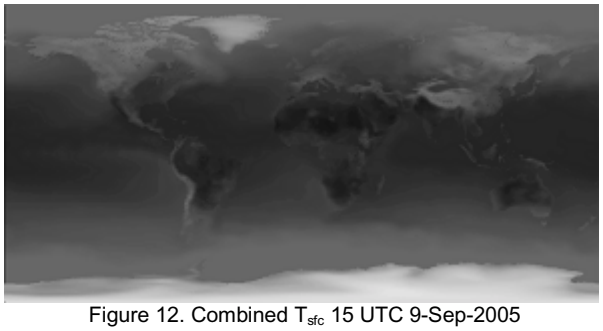

Figure 12. Combined T_{sfc} 15 UTC 9-Sep-2005

The global image of T_{sfc} was combined with a mosaic of global 11 μm data (See Figure 13) generating a single image T_{sfc}-T_{ir} (See Figure 14). We then again compared various T_{sfc}-T_{ir} and T_{ir} cloud/no cloud masks applied to the global mosaic of 11 μm data (See Figures 15-20).

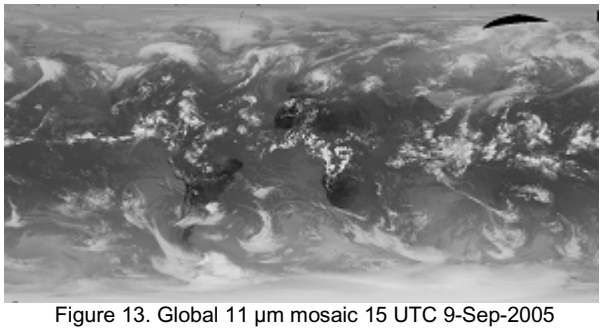

Figure 13. Global 11 μm mosaic 15 UTC 9-Sep-2005

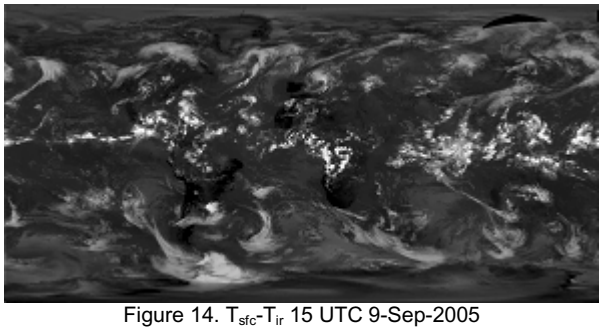

Figure 14. T_{sfc}-T_{ir} 15 UTC 9-Sep-2005

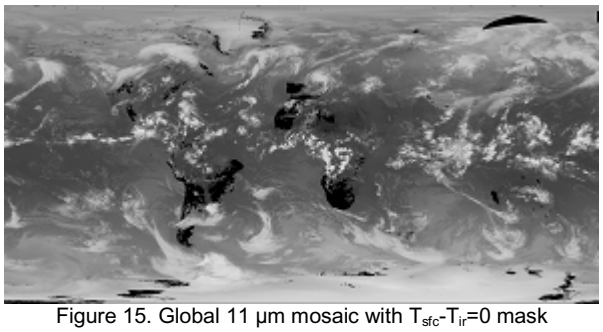

Figure 15. Global 11 μm mosaic with T_{sfc}-T_{ir}=0 mask

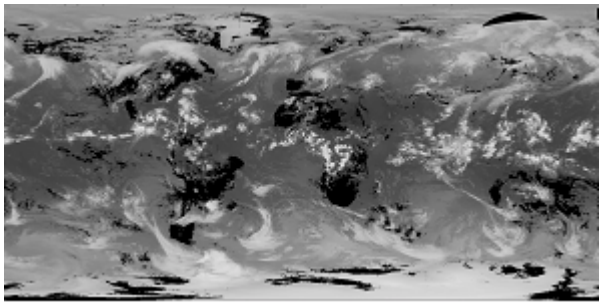

Figure 16. Global 11 µm mosaic with T_{sfc}-T_{ir}=4 mask

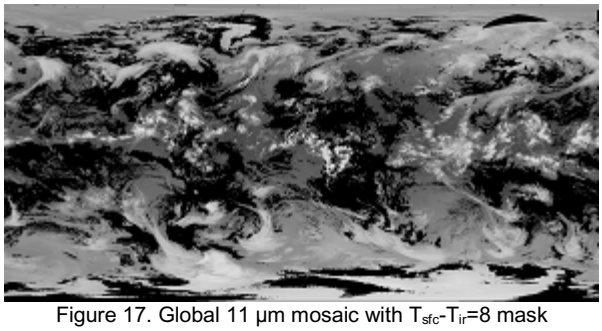

Figure 17. Global 11 µm mosaic with T_{sfc}-T_{ir}=8 mask

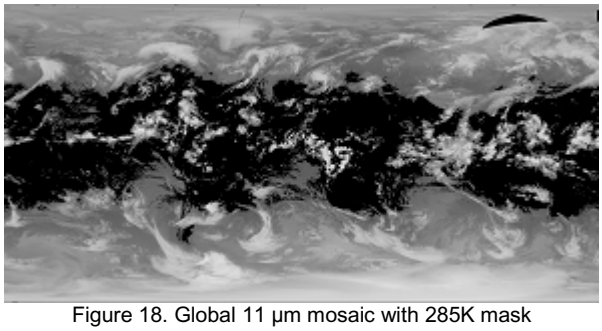

Figure 18. Global 11 µm mosaic with 285K mask

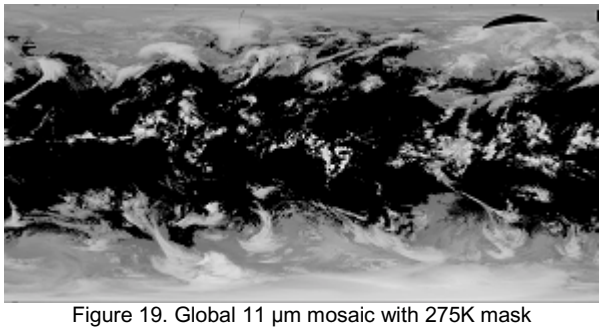

Figure 19. Global 11 µm mosaic with 275K mask

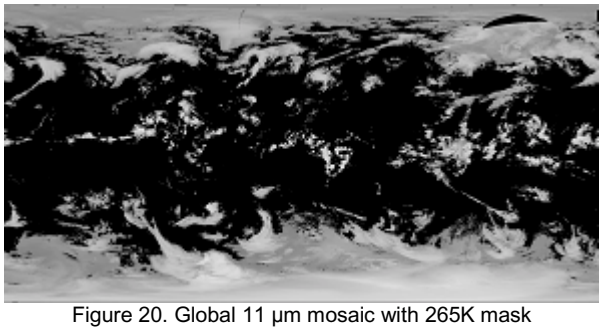

Figure 20. Global 11 µm mosaic with 265K mask

Temperature difference again shows better results than that of a single infrared temperature threshold. Even on the global scale, T_{sfc}-T_{ir}=8 is the best of the three difference masks. These results held through all of the several cases examined.

4. Cloud Transparency

To combine the global 11 µm mosaic with a basemap, we derived two T_{sfc}-T_{ir} based transparency equations. The first equation defines the opacity of the 11 µm image below the cloud/no cloud threshold:

$$\text{opacity} = 100 * \tan^{-1}\{ [(2.47 * (T_{sfc}-T_{ir}) - 20) + \pi/2] / \pi \}.$$

The constant 2.47 was empirically derived to make both equations equal for an opacity of 40%. The second equation defines the opacity of the 11 µm image greater than or equal to the cloud/no cloud threshold:

$$\text{opacity} = 100 * \{ \sin(\pi/2 * (T_{sfc} - T_{ir} - 7) / 110) \}^{-6}.$$

These equations are shown graphically in figure 21.

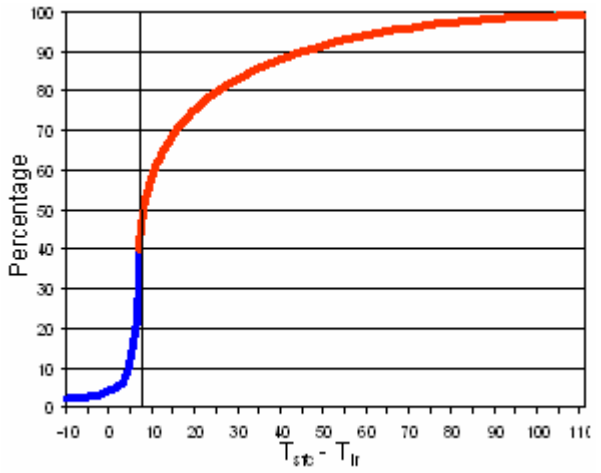

Figure 21. 11 µm mosaic percentage vs T_{sfc}-T_{ir}

Using the above equations, we combine the 11 µm global mosaic with NASA's Big Blue Marble imagery (See Figure 22) to generate the final product seen in figure 23.

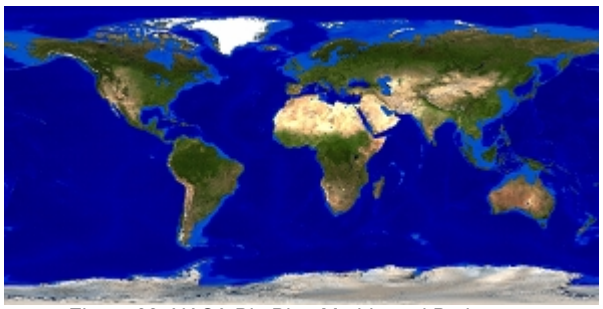

Figure 22. NASA Big Blue Marble and Bathymetry

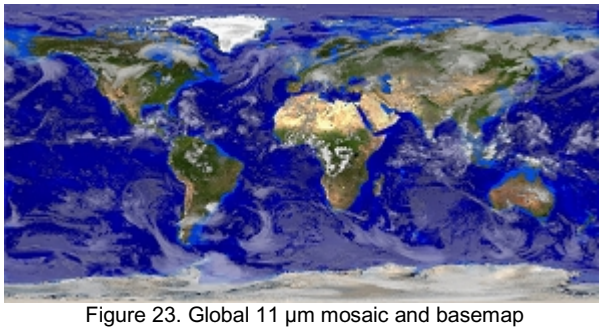

Figure 23. Global 11 µm mosaic and basemap

5. Future Endeavors

When attempting to increase the frequency of our global products from 6-hourly to 3-hourly, we found that decreased number of surface observations for 3,9,15 and 21 UTC produced poor analyses of T_{sfc}. Sample cases have been conducted substituting NCEP Global Forecasting System (GFS) model data for land based observational temperatures. Model data removes the worries of bad surface observations and data void areas from corrupting the analysis of T_{sfc}. Additional case studies are needed to judge the impact of model data on this algorithm, especially over ocean regions where temperature differences of up to 20 degrees were observed when comparing GFS and SST data.

Further, we have identified two situations where improvements can be made to this algorithm. First, an unexpected artifact was found to occur shortly after sunset when T_{ir} cools faster than $T_{sfc.}$ The rapid cooling of the ground increases T_{sfc}-T_{ir} resulting in an overestimation of cloud coverage. This artifact is most evident when there is a strong temperature inversion. A day/time based temperature difference offset may correct for this problem. Second, fog can exhibit extremely small values of T_{sfc}-T_{ir}, creating an underestimation of cloud coverage. Adding relative humidity information into the transparency calculation may improve the depiction of fog.

6. Blending Visible and Infrared Imagery

An experimental product that blends visible, infrared and basemap imagery is currently being used by the Cooperative Institute for Meteorological Satellite Studies (CIMSS) tropical cyclone group. Let t_i be the time of the image, t_o be the time of local noon, L be the length of the day and d be a weighting factor. The relationship between visible and infrared is set as follows. From sunrise to sunset

$$vis = 80 * [\sin (d * \pi/2)]^2$$

and

$$ir = 100 - vis$$

where

$$d = | t_i - t_o | / (L / 2).$$

After sunset and before sunrise

$$vis = 0.$$

These equations are shown graphically in figure 24.

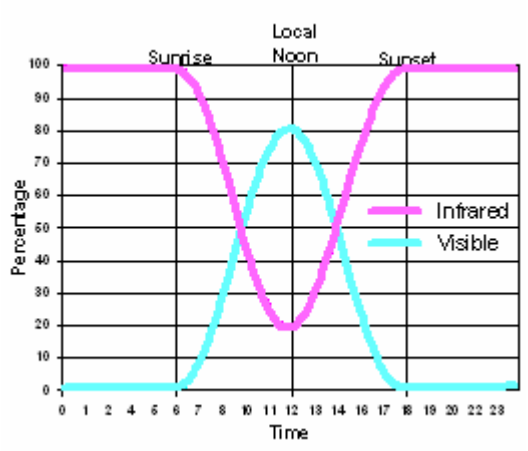

Figure 24. Visible and Infrared % vs Time

Further, cloud transparencies are based upon infrared brightness temperature and visible reflectance values, where cloud opacity increases as visible reflectance increases and infrared brightness temperatures decrease. A sample case uses GOES-12 visible (See Figure 25) and infrared (See Figure 26) imagery of hurricane Katrina from 28-Aug-2005 at 20:45 UTC. We calculate the following values for sunrise, sunset, visible weight and infrared weight of 11:34, 00:20, 48% and 52% respectively. The blended image is shown in Figure 27.

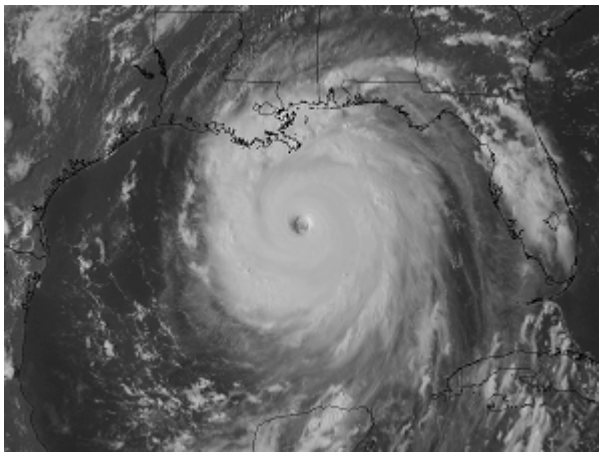

Figure 25. GOES-12 Visible 20:45 UTC 26-Aug-2005

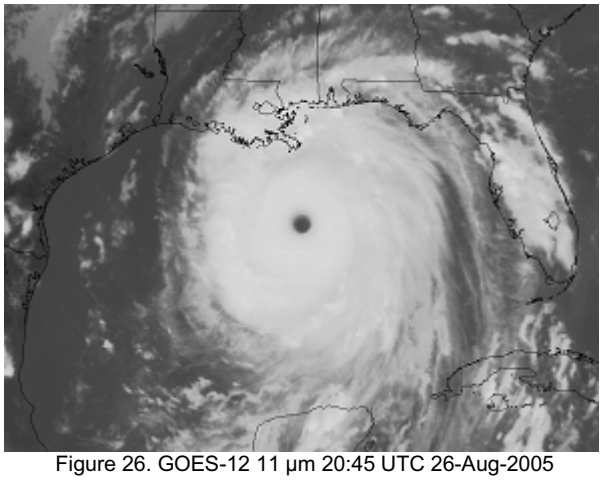

Figure 26. GOES-12 11 μm 20:45 UTC 26-Aug-2005

Figure 27. Blended visible and infrared

6. Conclusions

For the past few decades, the television media have done an exceptional job of using computer graphics to present current and forecasted weather conditions to the general public. Even the presentation of satellite imagery has improved by incorporating a variety of new basemaps. The one constant that has remained is the use of a single infrared temperature cloud/no cloud mask. The simple algorithms discussed in this paper offer two new techniques to greatly improve the depiction of clouds over basemaps, providing the media an alternative to existing graphics.

7. References

Lazzara, M. A., J. M. Benson, R. J. Fox, D. J. Laitsch, J. P. Rueden, D. A. Santek, D. M. Wade, T. M. Whittaker, and J. T. Young, 1999: The Man computer Interactive Data Access System: 25 years of interactive processing. *Bull. Amer. Meteor. Soc.,* **80**, 271-284.

Reynolds, R. W., 1988: A real-time global sea-surface temperature analysis. *J. Climate,* **1,** 75–86.

Reynolds, R. W., and D. C. Marsico, 1993: An improved real-time global temperature analysis. *J. Climate,* **6,** 114–119.